First-principles molecular-dynamics simulation of expanded liquid rubidium

Fuyuki Shimojo

Faculty of Integrated Arts and Sciences, Hiroshima University, Higashi-Hiroshima 739, Japan

Y. Zempo

Sumitomo Chemical, 6 Kitahara, Tsukuba 300-32, Japan

Kozo Hoshino and Mitsuo Watabe

Faculty of Integrated Arts and Sciences, Hiroshima University, Higashi-Hiroshima 739, Japan

The structural and electronic properties of expanded liquid rubidium are studied at 350 K, near the triple point, and 1400 K by means of a first-principles molecular-dynamics (MD) simulation, where the Kohn-Sham energy functional is minimized for each ionic configuration of the MD step using the preconditioned conjugate-gradient method. The results for the static structure at both temperatures and the diffusion coefficient near the triple point are in good agreement with experiments. While near the triple point the electron density $\rho(\mathbf{r})$ spreads over whole space, at high temperature $\rho(\mathbf{r})$ tends to localize due to a large spatial fluctuation of atomic density. The electron-ion correlation function is calculated using $\rho(\mathbf{r})$ and its temperature dependence is discussed.

I. INTRODUCTION

Interest in the study of structural, dynamic, and electronic properties of liquid alkali metals arises from the following two points: (1) collective behavior of ions immersed in the sea of electrons, and (2) the correlation between conduction electrons and the highly disordered state of ions. The dynamic properties of liquid alkali metals have been extensively investigated by means of classical computer simulations[1,2] and approximate theories[3] to complement recent experimental progress.[4-7] We have also studied the dynamic correlation functions and the associated memory functions of liquid sodium by means of a molecular-dynamics (MD) simulation[8] and a mode-mode coupling theory.[9] However, these theoretical studies used the effective pair potentials for ions based on the pseudopotential theory, where the interaction between conduction electrons and ions is treated by second order perturbation. Thus ion-ion correlation functions were discussed, but not electron-ion correlations.

However, the recent remarkable progress in theoretical studies of electron states of condensed matter makes it possible to combine the electronic structure calculation and the MD simulation. Since the pioneering theory was invented by Car and Parrinello,[10] various theoretical methods have been proposed.[11] In almost all studies using these methods, which are often called first-principles or *ab initio* MD simulation, the electronic structure is calculated within the Born-Oppenheimer approximation which separates the degrees of freedom of ions and electrons. Typically the plane-wave pseudopotential formulation is used, within the local density approximation to density functional theory. Since the forces acting on ions are calculated from first principles via the Hellmann-Feynman theorem, ionic trajectories are obtained nonem-

pirically. In principle, we can numerically investigate the correlations between the electronic structure, such as electron density distribution, and the disordered ionic configuration in liquid metals.

For liquid alkali metals, several first-principles dynamic simulations have been reported. Qian *et al.*[12] first calculated the activation energy for self-diffusion in liquid sodium, using the Car and Parrinello method.[10] They showed that the coefficient of self-diffusion and the activation energy were in good agreement with the experimental values. Bylander and Kleinman[13] also performed a first-principles MD simulation for liquid sodium, using an iterative technique for the electronic structure calculation rather than the Car-Parrinello method. They obtained the diffusion coefficient and pressure as a function of the temperature and volume. Theihaber[14] presented a scheme for dynamic simulation based on time-dependent density functional theory, and used it for calculating various properties of solid and liquid sodium. Lynch *et al.*[15] have computed the pair distribution functions and the diffusion coefficient for liquid lithium, sodium, and potassium, using the semiempirical extended Hückel method as well as using the local density functional theory. Foley, Smargiassi, and Madden[16] have calculated the dynamic structure factor of liquid sodium based on a modified Car-Parrinello method using an orbital-free density functional. More recently, Cabral and Martins[17] have simulated several states of liquid rubidium and cesium with first-principles MD, which is similar to the method used in this paper. They have found that the pair distribution functions and the diffusion coefficients obtained in the simulations are in good agreement with experiments.

In the present paper, we report on the results of our first-principles MD simulation for expanded liquid rubidium. The purposes of this paper are as follows: (i) to ob-

tain the static and dynamic ion-ion correlation functions of liquid rubidium from first-principles calculation, (ii) to compare the structural results obtained by our simulation with the neutron scattering experiment,[18] and (iii) to elucidate the relation of the electronic structure to the characteristic features of ionic structure of expanded liquid metals along the liquid-vapor coexistence curve.

There are two reasons to study liquid rubidium. (1) Among expanded liquid alkali metals, liquid rubidium has been studied by experiments most extensively. Neutron scattering experiments[6,18] reporting the static and dynamic structure factors have been performed over a wide range of temperatures from the triple point up to the liquid-vapor critical point. (2) Expanded liquid rubidium has been extensively studied theoretically by classical simulations[19-21] and approximate theories,[22] and so we can compare our results with those results.

In Sec. II the method of first-principles MD simulation used here is briefly described, with more details appearing in the Appendix. The results of our simulation and discussions are given in Sec. III. Finally, Sec. IV summarizes our work.

II. METHOD OF CALCULATION

According to density functional theory,[23] the total ground-state energy of a system of interacting electrons and ions is a unique functional of the electron density $\rho(\mathbf{r})$. In terms of occupied Kohn-Sham (KS) orbital $\psi_m(\mathbf{r})$, the charge density $\rho(\mathbf{r})$ can be expressed by

$$\rho(\mathbf{r}) = 2\sum_m^{occ} f_m|\psi_m(\mathbf{r})|^2, \tag{1}$$

where f_m is an occupation number of the mth state, and the factor of 2 stands for double-spin occupancy. The KS total-energy functional can be written as

$$E[\{\psi_m\}, \{\mathbf{R}_I\}, \{f_m\}] = 2\sum_m^{occ} f_m\left(\int \psi_m^*(\mathbf{r})\left[-\frac{1}{2}\nabla^2\right]\psi_m(\mathbf{r})d\mathbf{r} + \int \psi_m^*(\mathbf{r})V_{ext}(\mathbf{r})\psi_m(\mathbf{r})d\mathbf{r}\right)$$
$$+ \frac{1}{2}\int \frac{\rho(\mathbf{r})\rho(\mathbf{r}')}{|\mathbf{r} - \mathbf{r}'|}d\mathbf{r}\,d\mathbf{r}' + E_{xc}[\rho] + \frac{1}{2}\sum_{I\neq J}\frac{Z_I Z_J}{|\mathbf{R}_I - \mathbf{R}_J|}, \tag{2}$$

where $V_{ext}(\mathbf{r})$ is an external potential, $E_{xc}[\rho]$ the exchange-correlation functional, and Z_I the valence of the Ith ion. Only the minimum value of the KS energy functional has physical meaning.[23] At the minimum, the KS energy functional is equal to the ground-state energy of the system of electrons with ions in position $\{\mathbf{R}_I\}$.

In our simulation, the KS energy functional is minimized after each MD step using an iterative scheme based on the preconditioned conjugate-gradient method. This type of MD simulation is usually called conjugate-gradient molecular dynamics (CG-MD), which was recently developed by several authors.[24-28] While some au-

thors employ a band-by-band scheme, we use the all-band technique in our calculation, because it provides rapid convergence and consists of several simple steps.[29,30] For preconditioning, we use a modified version of Fukumoto's method.[31]

In applying the first-principles MD simulation to liquid metals, the fractional occupancy of each state must be taken into account, as was introduced by Gillan.[32] When the variable occupation numbers are explicitly included, it is required that an additional term be added to the energy functional:[33,34]

$$F[\{\psi_m\}, \{\mathbf{R}_I\}, \{f_m\}] = E[\{\psi_m\}, \{\mathbf{R}_I\}, \{f_m\}] + \Delta E$$
$$= E[\{\psi_m\}, \{\mathbf{R}_I\}, \{f_m\}] + k_B T_{el}\sum_m \{f_m \ln f_m + (1 - f_m)\ln(1 - f_m)\}, \tag{3}$$

where E is the Kohn-Sham energy functional Eq. (2), k_B the Boltzmann constant, T_{el} the Fermi temperature, and f_m the fractional occupation number of the one-electron state ψ_m. We minimize this functional, taking into account the effect of the fractional occupation.

Though Eq. (3) is formally the same as the free energy in finite temperature density functional theory,[35] the additional term ΔE is introduced so as to make the energy functional behave properly when fractional occupancies are allowed and, therefore, ΔE and T_{el} should be considered as disposable parameters rather than physical quantities.[33]

In this calculation we use the norm-conserving pseu-

dopotential proposed by Troullier and Martins.[36] The s component is treated as a local potential, while the p component is treated as a nonlocal potential using the Kleinman and Bylander form.[37] For the exchange-correlation functional, the parametrized form of Perdew and Zunger is employed.[38] The core corrections[39] are not considered in our simulations.

Using the Nosé-Hoover thermostat technique,[40,41] the equations of motion are solved via the velocity Verlet algorithm with time step $\Delta t = 2.4 \times 10^{-15}$ s. The supercell contains 54 rubidium atoms with periodic boundary conditions. Two simulations are carried out at different densities along the liquid-vapor coexistence curve: one

at 1.459 g/cm³ and 350 K near the triple point and the other at 0.970 g/cm³ and relatively higher temperature 1400 K. These densities correspond to supercell sizes of L = 17.38 and 19.92 Å, respectively. Only Bloch functions at the Γ point are used and the KS orbitals are expanded in plane waves with an energy cutoff of 6 Ry, which leads to 8829 and 13 205 plane waves at 350 K and 1400 K, respectively.

The electronic energy minimization by the all-band conjugate-gradient method is terminated after the quantity $|(F^{(n+1)} - F^{(n)})|/|F^{(n)}|$ becomes smaller than 10^{-6}, where n is the iteration number. However, at higher temperature, the convergence rate of the energy functional becomes worse due to the large displacements of ionic positions. This difficulty comes from the difference of the length of the gradient vector for each band, which is defined as

$$g_m^{(n)} = -(H - \varepsilon_m^{(n)})\psi_m^{(n)}. \qquad (4)$$

In reported all-band calculations, the preconditioner can adjust the length of each $g_m^{(n)}$ to the same order as well as change the direction of each $g_m^{(n)}$ to point to the minimum of the energy functional. In disordered systems, especially in liquid metals, it sometimes happens that the wave functions of a few bands are far from their respective eigenfunctions. In order to solve this problem, we employ a combination of the all-band method and the band-by-band method. For each all-band iteration, an additional specified band minimization is carried out so that errors of all bands are of the same order. Using this stabilizing procedure, our CG-MD technique is well suited to calculate the electronic structure of disordered systems. From near the triple point up to the critical point, our calculation is quite stable.

In any CG-MD simulation, the initial charge density is also important. In our calculation, it is estimated by extrapolating the charge density at previous steps.[28] Moreover, the initial wave functions are estimated from the wave functions at previous steps by subspace diagonalization.[26,27]

As an initial configuration of ions for first-principles MD simulation at each temperature, we use the final result of a classical MD simulation based on the effective pair potential generated from the pseudopotential perturbation theory. The system is equilibrated during the initial 1 ps in every simulation. The quantities of interest are obtained by averaging over about 3 ps after this equilibration. During the simulations, the conserved quantities in the Nosé-Hoover dynamics are kept constant with fluctuation being less than 1 mRy.

III. RESULTS AND DISCUSSION

A. Pair distribution function

In Figs. 1(a) and 1(b), we compare the calculated pair distribution functions $g(r)$ at 350 and 1400 K, respectively, with the experimental results.[18,42] The calculation of $g(r)$ is extended up to distances equal to the half-diagonal of the supercells.[43] From these figures, we see
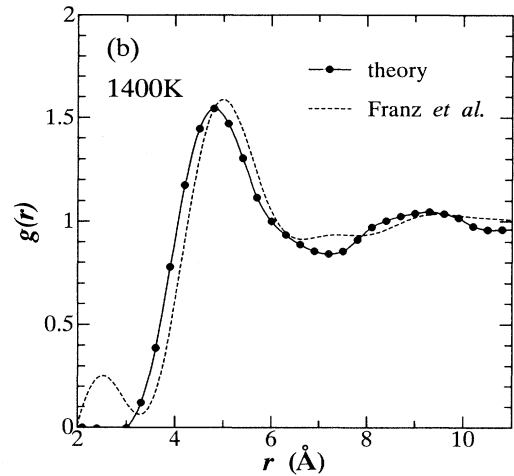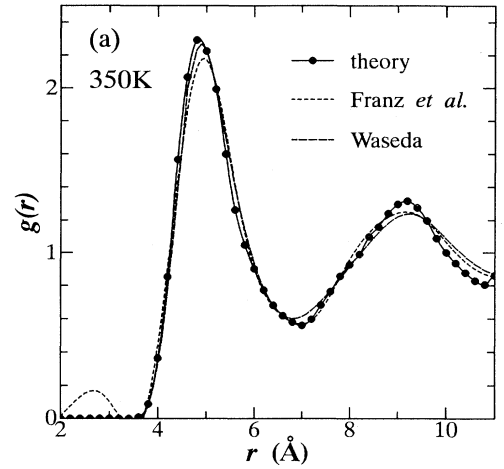
FIG. 1. Pair distribution functions $g(r)$ at 350 K (a) and 1400 K (b). Solid line shows $g(r)$ obtained by this calculation, and the dashed and dotted lines show the experimental results of Franz et al. (Ref. 18) and Waseda (Ref. 42), respectively.
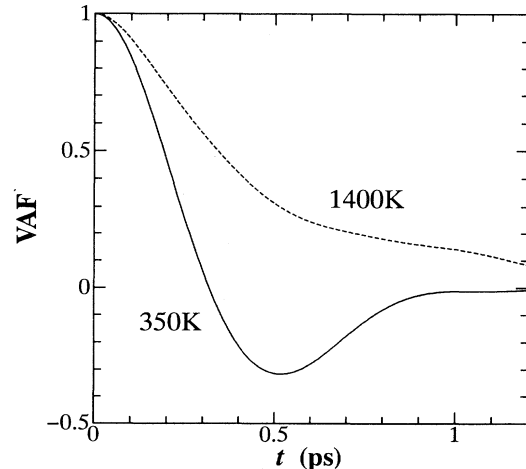
FIG. 2. Velocity autocorrelation functions at 350 K (solid line) and 1400 K (dashed line).
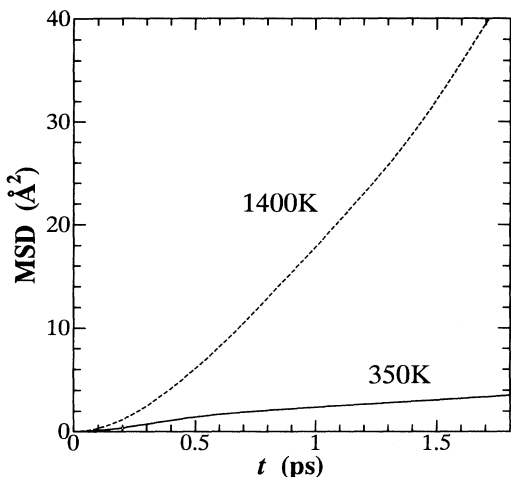
FIG. 3. Mean square displacements at 350 K (solid line) and 1400 K (dashed line).

that the calculated results are in good agreement with the experimental results, which means that we have succeeded in reproducing the structure of liquid rubidium for a wide range of temperatures. The features observed in $g(r)$ are as follows. The average nearest-neighbor distance, namely, the position of the first peak of $g(r)$, does not change with decreasing density. On the other hand, the coordination number N_1, which is defined by $2\rho \int_0^{r_1} 4\pi r^2 g(r)dr$ with r_1 being the position of the first peak of $g(r)$, decreases from 8.0 at 350 K to 4.8 at 1400 K. These features are observed for rubidium[18] and cesium[6] experimentally. It has also been shown theoretically that these characteristic features are common to all expanded liquid alkali metals.[22]

B. Dynamic properties of ions

We are interested in atomic dynamics in liquid rubidium, and so we calculate the velocity autocorrela-

(a)

(b)

(c)

(d)
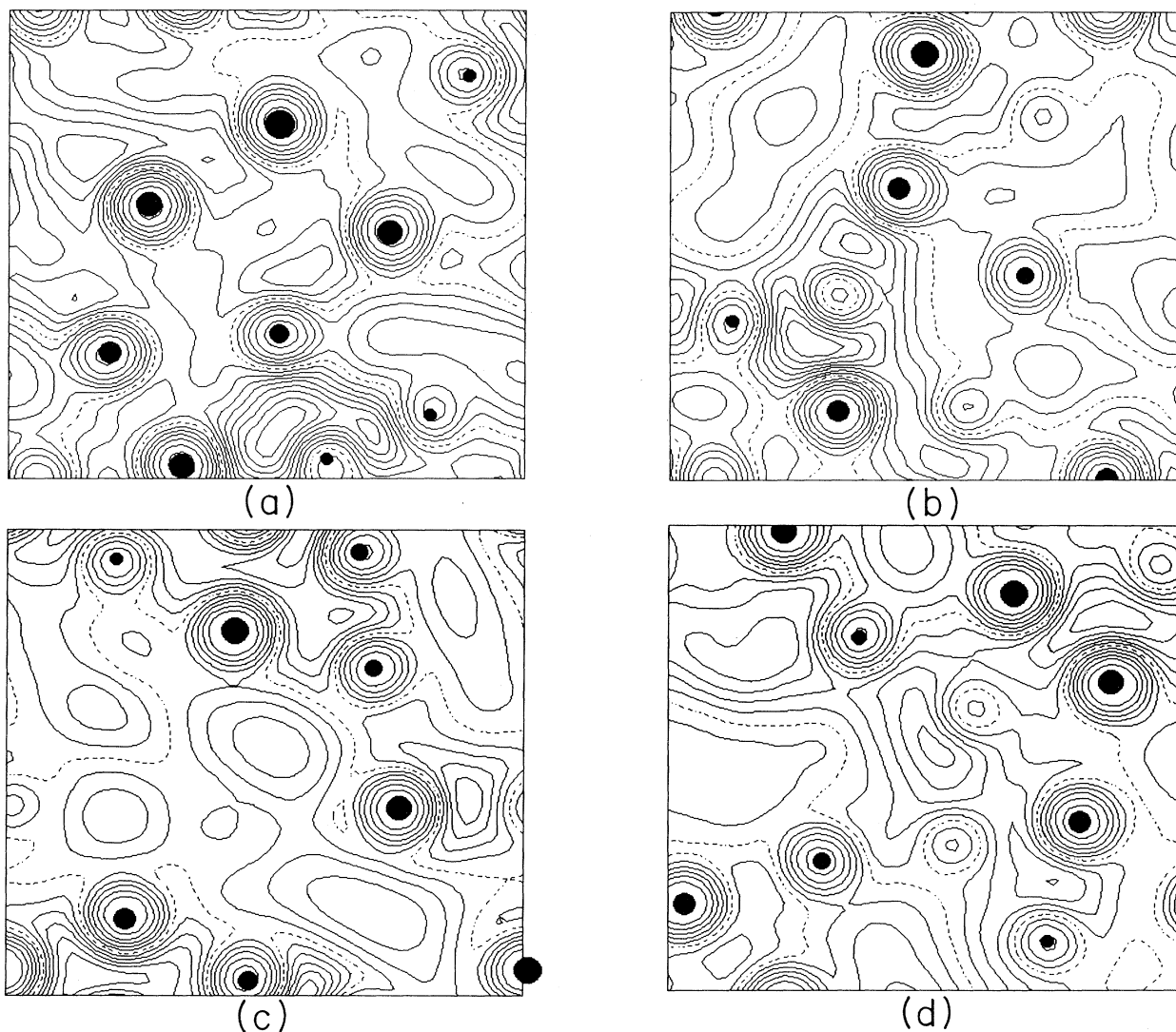
FIG. 4. Contour plots of the valence electron density distribution $\rho(\mathbf{r})$ at 350 K. The supercell is cut by four parallel planes with equal distance, and $\rho(\mathbf{r})$ on the planes are plotted. The contour lines are drawn in interval, 2×10^{-4} a.u. The dashed lines mean $\bar{\rho} = 1.5 \times 10^{-3}$ a.u.

tion function (VAF) and the mean square displacement (MSD), which are shown in Figs. 2 and 3, respectively. From Fig. 2, it is seen that the VAF at 350 K shows an oscillating behavior, while it decreases monotonically at 1400 K. The oscillating behavior of VAF near the triple point was also observed in the classical MD simulation by Tanaka,[20] although his result showed that the amplitude of oscillation is smaller and the oscillation continues to longer time than the present VAF. The self-diffusion coefficient D is one of the most important transport coefficients, and can be obtained from the integration of VAF or from the slope of MSD in a long time region, where MSD is proportional to $6Dt$. The values of D obtained at 350 K are 2.4×10^{-5} and 2.6×10^{-5} cm^2/s from MSD and VAF, respectively, which are in reasonable agreement with the experimental value 2.5–3.8 $\times 10^{-5}$ cm^2/s.[44]

Near the triple point each rubidium ion is surrounded by a "cage" of other ions, the members of which remain the same for a relatively long time interval, like ions in a solid. Each ion shows thermal vibrating motion in the cage, which causes the vibrating behavior of VAF as displayed in Fig. 2. On the other hand, at 1400 K, we can expect rubidium ions to move more freely, because the vibrating behavior of VAF is absent and the large diffusion is observed in MSD. It should be noted, however, that we can see highly correlated motion of ions even at 1400 K from trajectories of ions. The discussions of the atomic dynamics related to the electron density distribution will be presented in the next subsection.

C. Electron density distribution

Figures 4 and 5 show snapshots of contour plots of the pseudovalence electron density distributions $\rho(\mathbf{r})$ at 350
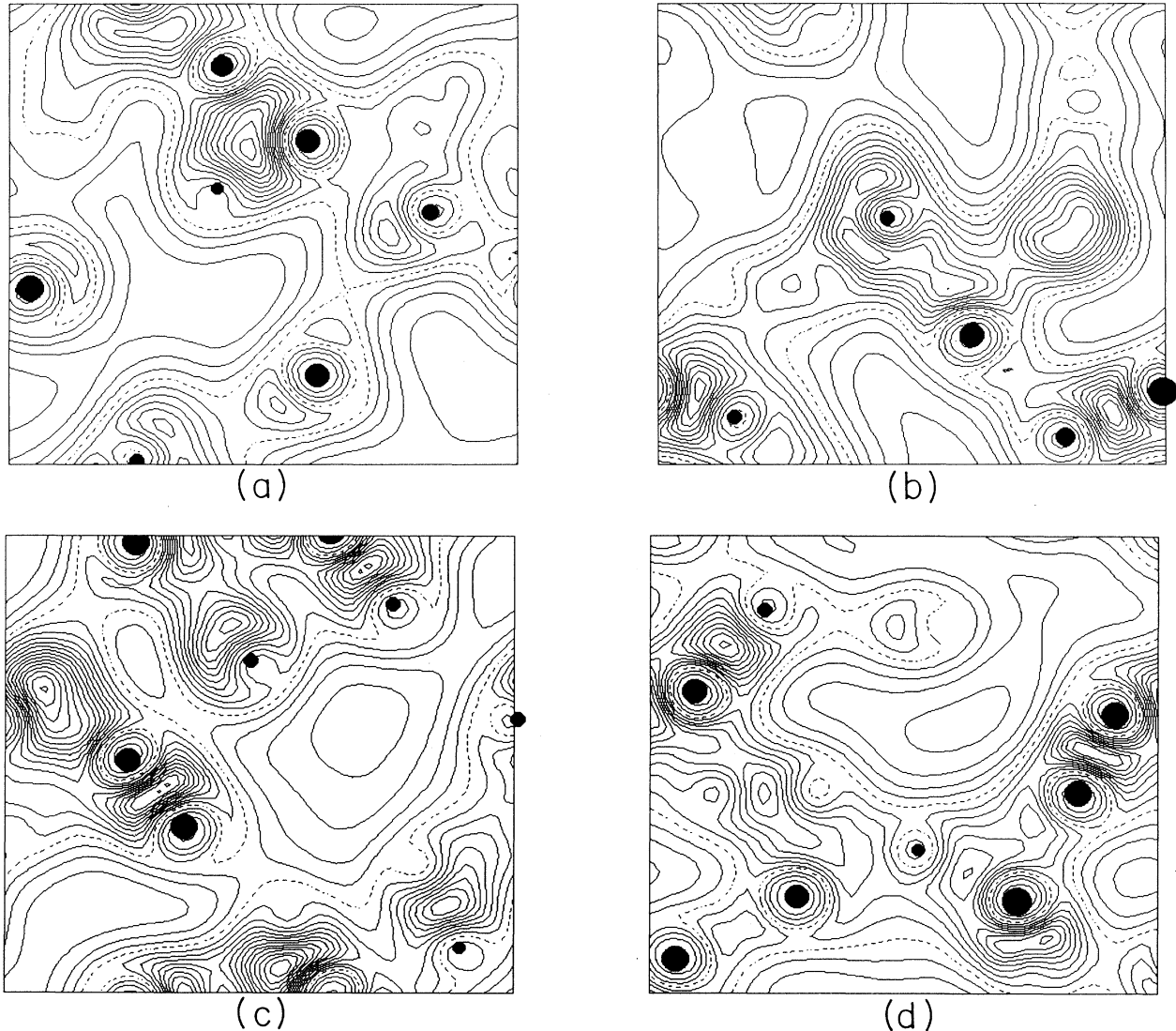
FIG. 5. Contour plots of the valence electron density distribution $\rho(\mathbf{r})$ at 1400 K. The supercell is cut by four parallel planes with equal distance, and $\rho(\mathbf{r})$ on the planes are plotted. The contour lines are drawn in interval, 2×10^{-4} a.u. The dashed lines mean $\bar{\rho} = 1 \times 10^{-3}$ a.u.

and 1400 K, respectively. The supercell is cut by four parallel planes with equal distance, and $\rho(\mathbf{r})$ on these planes are plotted from the bottom (a) to the top (d) of the supercell. The contour lines are drawn in intervals of 2×10^{-4} a.u. in both figures. The dashed lines mean the average electron density $\overline{\rho} = N_{\text{el}}/V = 1.5 \times 10^{-3}$ and 1×10^{-3} a.u. in Figs. 4 and 5, respectively, where N_{el} is the number of electrons and V the volume.

As expected, we see from the figures that the fluctuation of atomic density becomes large with increasing temperature, that is, the rubidium ions distribute homogeneously at 350 K, while at 1400 K there are wide areas where no ions are found, and the ions distribute in other areas. It is also found that the valence electron density distribution $\rho(\mathbf{r})$ at high temperature is very different from that near the triple point. As shown in Fig.

4, near the triple point $\rho(\mathbf{r})$ spreads over all space except in the neighborhood of atomic positions, since the core states are not taken into account in $\rho(\mathbf{r})$. On the other hand, at high temperature $\rho(\mathbf{r})$ tends to localize due to the large spatial fluctuation of atomic density. Figure 5 shows that the electronic charge piles up in the areas where the ions come together, which are recognized by dense contour lines.

In order to clarify the change in $\rho(\mathbf{r})$ with increasing temperature, we calculate an artificial electron density $\rho^a(\mathbf{r})$ by superposing the pseudovalence electron densities obtained from the pseudized atomic $5s$ wave function, and obtain the difference $\delta\rho(\mathbf{r}) = \rho(\mathbf{r}) - \rho^a(\mathbf{r})$ as shown in Figs. 6 and 7, where contours are plotted for $\delta\rho(\mathbf{r}) > 0$ since the areas for $\delta\rho(\mathbf{r}) < 0$ are only near the atomic positions and drawing contours in these areas

(a)   (b)

(c)   (d)
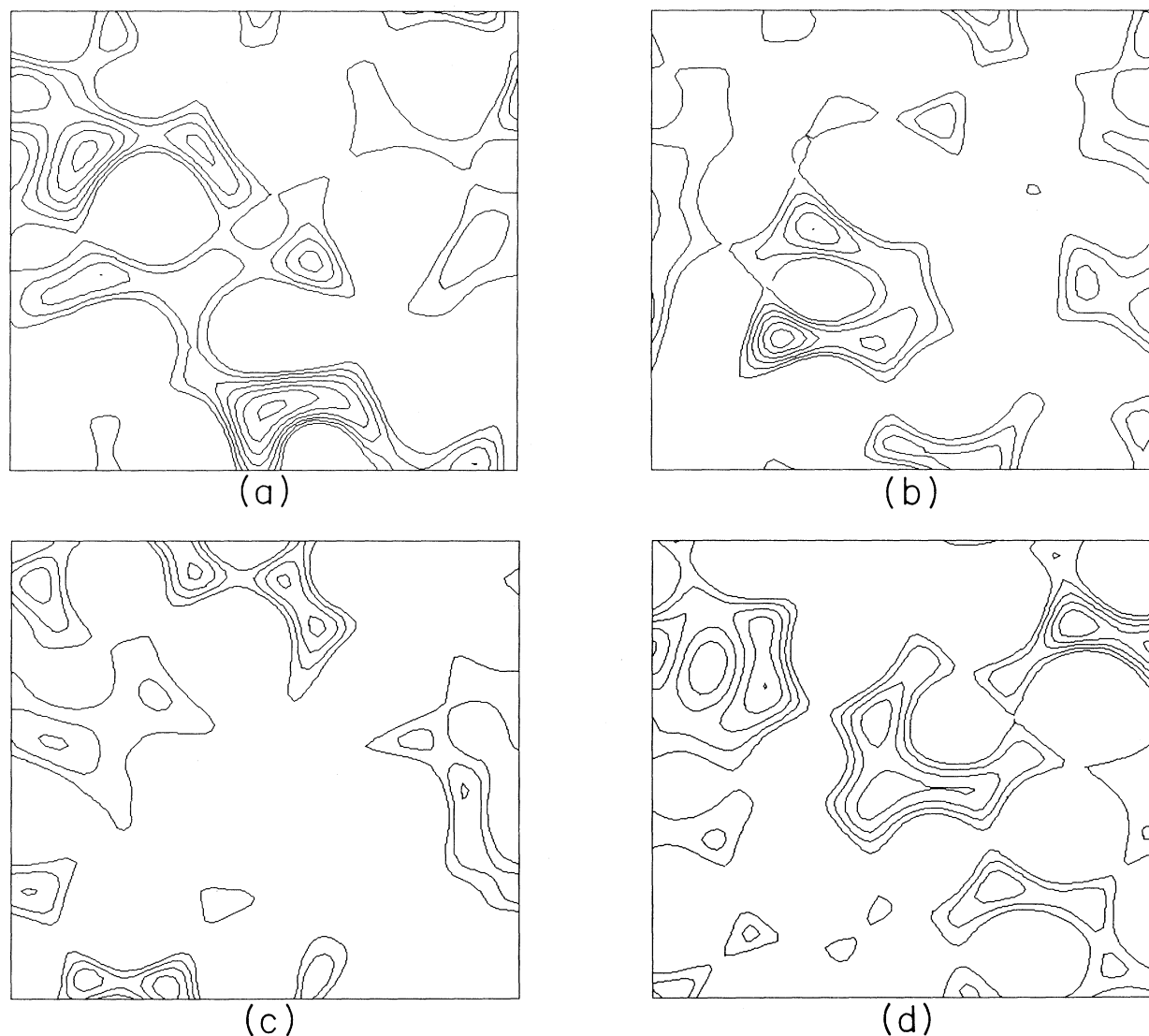
FIG. 6. Contour plots of the difference, $\delta\rho(\mathbf{r}) = \rho(\mathbf{r}) - \rho^a(\mathbf{r})$, at 350 K, where $\rho(\mathbf{r})$ is the valence electron density obtained self-consistently and $\rho^a(\mathbf{r})$ is an artificial electron density obtained by superposing the atomic $5s$ electron densities. The contour lines are plotted for $\delta\rho(\mathbf{r}) > 0$ with interval, 1×10^{-4} a.u.

makes the figures confusing. The contour lines are drawn in intervals of 1×10^{-4} a.u. By comparing Fig. 6 with Fig. 7, it is seen that $\delta\rho(\mathbf{r})$ at 350 K spreads and has small values, while $\delta\rho(\mathbf{r})$ at 1400 K are extremely large [indicating a large $\rho(\mathbf{r})$ as shown in Fig. 5] in a narrow region, where a few ions come together.

It is interesting to discuss the electron density distributions as already shown in Figs. 4–7 in connection with atomic dynamics, which was discussed in the preceding subsection. Near the triple point, each rubidium ion in the liquid is surrounded by other ions, which seldom change. In $\rho(\mathbf{r})$, a homogeneous distribution is observed, and this distribution does not change much with time. On the other hand, at 1400 K, binarylike collisions at short distances are observed. We can see $\rho(\mathbf{r})$ at the instant of the collision in Figs. 5 and 7, that is, the extremely large $\delta\rho(\mathbf{r})$ and $\rho(\mathbf{r})$ between the two ions. The large inhomogeneity in $\rho(\mathbf{r})$ is not only caused by thermal fluctuations but is also related to the fact that there are few ions around a central ion with the distances of about 5 Å. The latter can be understood as follows. The values of $\rho(\mathbf{r})$ at 1400 K along the line between two ions with a distance of about 5 Å are almost the same as those at 350 K, which means the local electronic structure at high temperature is not different from that near the triple point. As the density decreases with increasing temperature, rubidium ions become surrounded by some ions at distances of about 5 Å in order to keep the local electronic energy low, which causes the decrease of the coordination number and the large inhomogeneity in $\rho(\mathbf{r})$.

D. Electron-ion correlation function

The correlation function between the valence electrons and ions is defined as
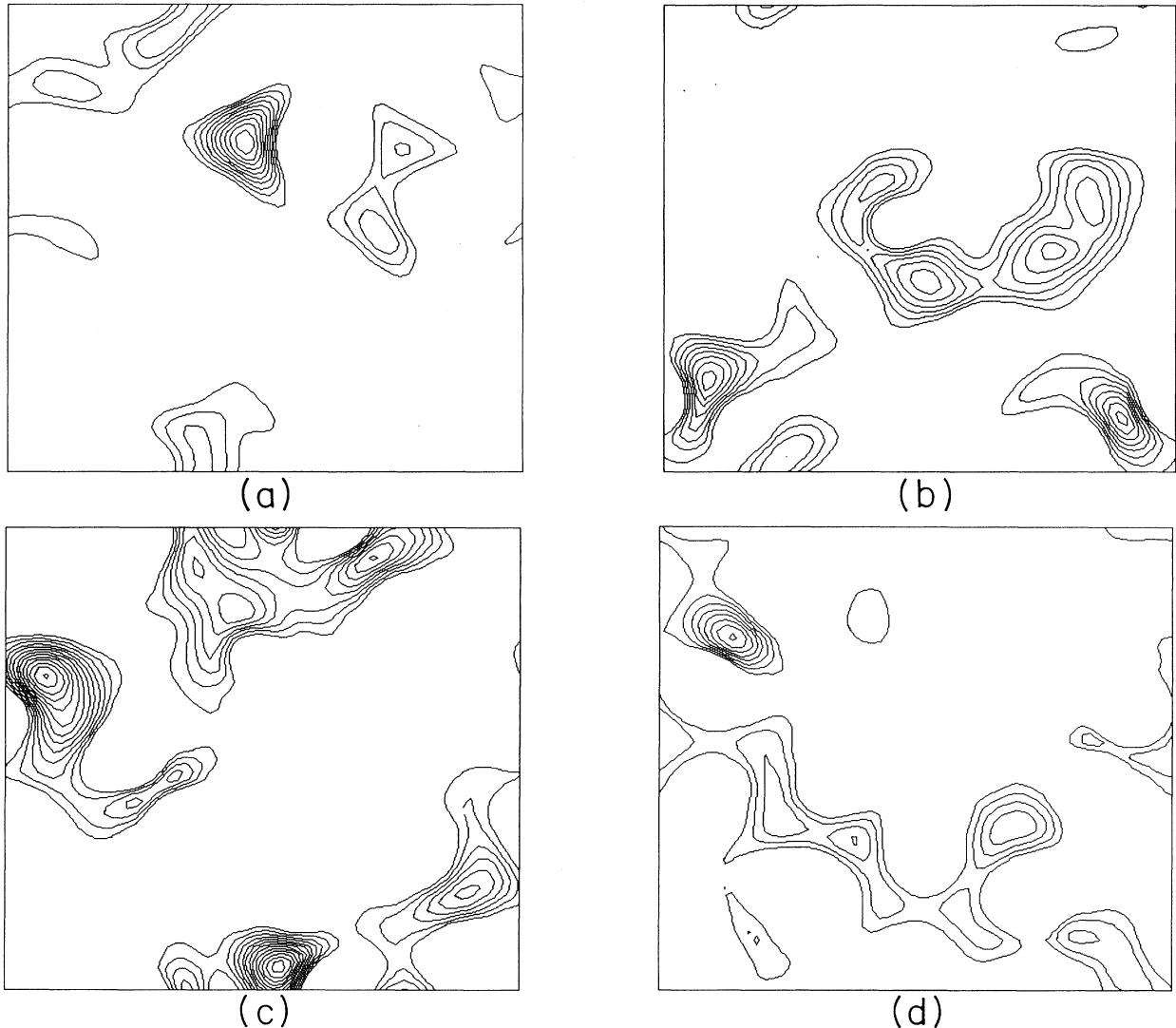
FIG. 7. Contour plots of the difference, $\delta\rho(\mathbf{r}) = \rho(\mathbf{r}) - \rho^a(\mathbf{r})$, at 1400 K. The contour lines are plotted for $\delta\rho(\mathbf{r}) > 0$ with interval, 1×10^{-4} a.u.

$$g_{ei}(r) = \frac{\langle n_{ei}(r) \rangle}{4\pi r^2 \bar{\rho} \Delta r} , \qquad (5)$$

where $\langle n_{ei}(r) \rangle$ is the average number of valence electrons in a spherical shell, centered on an ion at the origin, with a thickness Δr from $r - \Delta r/2$ to $r + \Delta r/2$. The brackets $\langle \cdots \rangle$ denote the average over all ions. The electron-ion correlation function $g_{ei}(r)$ is interesting not only theoretically but also experimentally, since it can be estimated by comparing the structure factor obtained by neutron scattering with that of x-ray scattering. Recently, two of us[45] calculated $g_{ei}(r)$ of liquid sodium near the triple point within the linear screening approximation based on the pseudopotential theory and discussed its characteristic features in comparison with the experimental results.[46]

In Fig. 8, we show the $g_{ei}(r)$ of the liquid rubidium at 350 K (solid line) and 1400 K (dashed line) calculated by Eq. (5) using the electron densities shown in the preceding section. At both temperatures, the position of the first peak of $g_{ei}(r)$ is about 2.1 Å, which corresponds to the middle point of the average distance between neighboring pairs of ions and is larger than the position of the peak of the atomic $5s$ electron density, 1.8 Å. It was also pointed out in the previous work[45] that the first peak of $g_{ei}(r)$ comes from the first peak of the screening charge density around an ion and the position of the first peak shifts outward in comparison with that of the atomic valence electron density. The position of the first minimum of $g_{ei}(r)$ is almost the same as that of the first peak of the ion-ion pair distribution function $g(r)$, since the valence electron density $\rho(\mathbf{r})$ does not include the core states and therefore has a low value in the core region of each ion.

As for the temperature dependence of $g_{ei}(r)$, we can see the following characteristic features: (i) The positions of the first peak and the first minimum of $g_{ei}(r)$ do not change with increasing temperature. This feature results from the fact that the position of the first peak of $g(r)$ of expanded liquid alkali metals does not change when the temperature is increased from the triple point to the
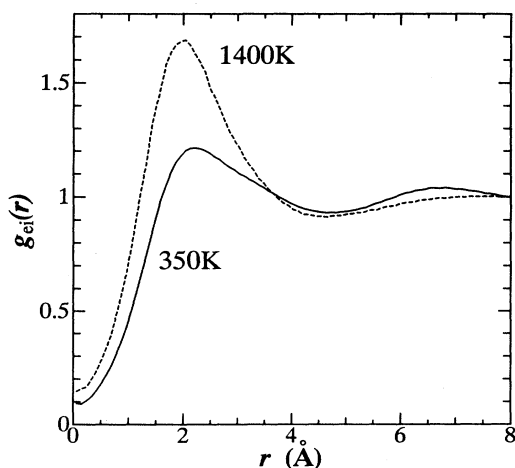
critical point along the liquid-vapor coexistence curve.[22] (ii) With increasing temperature, the first peak of $g_{ei}(r)$ becomes higher and the second peak becomes less clear, which suggests that the distribution of valence electrons is more localized between ions at higher temperature. (iii) The average number of valence electrons in a sphere, centered on an ion at the origin, with a radius r_{ei} can be estimated by $N_e(r_{ei}) = \int_0^{r_{ei}} 4\pi r^2 \bar{\rho} g_{ei}(r) dr$. If r_{ei} is taken to be r_{WS}, where r_{WS} is the radius of the effective Wigner-Seitz (WS) sphere and is equal to the electron-sphere radius r_s, then $N_e(r_{WS}) = 1.09$ and 1.37 at $T = 350$ K ($r_{WS} = 2.85$ Å) and $T = 1400$ K ($r_{WS} = 3.27$ Å), respectively. The radii $r_{ei}^{(1)}$ which give rise to $N_e(r_{ei}^{(1)}) = 1$ are almost the same irrespective of temperature, i.e., 2.8 Å at 350 K and 2.9 Å at 1400 K, which are larger than the position of the first peak of $g_{ei}(r)$, 2.1 Å. While $r_{ei}^{(1)}$ is almost equal to r_{WS} near the triple point, $r_{ei}^{(1)}$ deviates from r_{WS} at higher temperature, on account of the localized nature of valence electrons due to a large spatial fluctuation of ionic density.

IV. SUMMARY

The temperature dependence of the structural and electronic properties of expanded liquid rubidium is studied by means of a first-principles molecular-dynamics simulation, in which the Kohn-Sham energy functional is minimized for each ionic configuration, using the iterative scheme based on the preconditioned conjugate-gradient method. Our simulations are carried out at 350 K, near the triple point, and 1400 K.

The radial distribution functions at both temperatures and the diffusion coefficient near the triple point are in good agreement with experiments. It is shown that while near the triple point, the electron density distribution $\rho(\mathbf{r})$ spreads over all space, at high temperature, $\rho(\mathbf{r})$ tends to localize due to the large spatial fluctuation of atomic density. Some discussions on the electron density distributions in connection with atomic dynamics are given. The electron-ion correlation function is calculated using $\rho(\mathbf{r})$ and the characteristic feature of its temperature dependence is discussed.

ACKNOWLEDGMENTS

FIG. 8. Electron-ion correlation functions $g_{ei}(r)$ at 350 K (solid line) and 1400 K (dashed line).

APPENDIX

In this appendix we describe the CG-MD scheme which was employed in the calculations presented in this paper. Probably the most well-known CG method in reciprocal space is the band-by-band type CG method developed

and successfully applied by Teter, Payne, and Allan.[24] One of the characteristic features of this method is the use of a simple preconditioning process in the minimization; i.e., the following matrix is applied to the steepest descent vector $g_m^{(n)}$:

$$K_{\mathbf{G},\mathbf{G}'}^{(n)} = \delta_{\mathbf{G},\mathbf{G}'} \frac{27 + 18x + 12x^2 + 8x^3}{27 + 18x + 12x^2 + 8x^3 + 16x^4} , \quad (A1)$$

where $x = \frac{1}{2}|\mathbf{k} + \mathbf{G}|^2/T_m^{(n)}$, and $T_m^{(n)} = f_m^{(n)}\langle \psi_m^{(n)}| -\frac{1}{2}\nabla^2| \psi_m^{(n)}\rangle$ is the kinetic energy of the state $\psi_m^{(n)}$. Keeping the wave function orthogonal to both the gradient and the conjugate direction, the band-by-band calculation has two steps; the local iteration to update a single band, and the global iteration. In each iteration, we need to calculate the nonlocal pseudopotential, which is the most time consuming part, and therefore it is expensive unless the separable form[13] is used in the pseudopotential calculation.

On the other hand, in an all-band calculation, an update procedure is simple in the sense that all of the wave functions are updated only by the global iteration. However, Fukumoto pointed out the difficulty of the above preconditioning process when we apply it to the all-band type calculation, because the length of each preconditioned $g_m^{(n)}$ is not of the same order. He proposed a simple modification of the preconditioner to improve the convergence of the all-band calculation,

$$\tilde{K}_{\mathbf{G},\mathbf{G}'}^{(n)} = \frac{K_{\mathbf{G},\mathbf{G}'}^{(n)}}{K_{\mathbf{G},\mathbf{G}'}^{(n)} + (1 - K_{\mathbf{G},\mathbf{G}'}^{(n)})T_m^{(n)}/\alpha} , \quad (A2)$$

where α is a scaling parameter.[31] In Eq. (A2), we use the average of the kinetic energy for α,

$$\alpha = \frac{2}{N}\sum_m^{occ} f_m^{(n)}\langle \psi_m^{(n)}| -\frac{1}{2}\nabla^2| \psi_m^{(n)}\rangle . \quad (A3)$$

The conjugate-gradient directions $h_m^{(n)}$ are given by

$$h_m^{(n)} = \tilde{K}^{(n)}g_m^{(n)} + \tilde{\beta}^{(n)}h_m^{(n-1)} , \quad (A4)$$

where the mixing ratio $\tilde{\beta}^{(n)}$ is taken as

$$\tilde{\beta}^{(n)} = \tanh\left(\frac{\sum_m f_m^{(n)}\langle g'^{(n)}_m| g'^{(n)}_m\rangle}{\sum_m f_m^{(n)}\langle g'^{(n-1)}_m| g'^{(n-1)}_m\rangle}\right)$$

and $\tilde{\beta}^{(0)} = 0$. (A5)

In this expression, $g'^{(n)}_m = \tilde{K}^{(n)}g_m^{(n)}$. It is necessary to maintain the value of $\tilde{\beta}^{(n)}$ to be less than unity using

this hyperbolic trigonometrical function, because we frequently come across numerical fluctuations in an all-band calculation, especially for a disordered system.[31]

The updated wave functions are given by

$$\psi_m^{(n+1)} = \mathcal{ON} [\psi_m^{(n)} + \lambda^{(n)}h_m^{(n)}], \quad (A6)$$

where $\mathcal{ON}$ is the normalization operator together with Gram-Schmidt orthogonalization, and the scalar $\lambda^{(n)}$ is obtained by a one-dimensional minimization along the orthonormal constraint line. In our energy minimization, the convergence of each band is checked. Although our CG is based on the all-band method, additional specific band minimization is applied to states which do not reach convergence. This minimization is carried out with a fixed Hamiltonian for the nth iteration. When we use the fractional occupation number $f_m^{(n)}$, it is necessary to obtain the eigenvalue $\varepsilon_m^{(n)}$, which is obtained from the diagonalization of the Hamiltonian matrix in the subspace spanned by the updating wave functions:

$$H_{ij} = \langle \psi_j^{(n)}|H|\psi_i^{(n)}\rangle. \quad (A7)$$

Using Eqs. (4), (A4), and (A6), the wave function and the potential are updated. This process guarantees the correct occupation number for each eigenstate. Besides, to avoid charge sloshing, we use Kerker's simple mixing scheme.[47] In our experience, it is quite sufficient, and more sophisticated schemes are not necessary.[48]

In the MD simulation, this CG energy minimization based on the all-band method is used for each MD step. In order to reduce the number of iterations in each minimization, we extrapolate the wave function for the initial guess at the next time step t_{n+1}, using the values of the wave functions at t_n and t_{n-1},

$$\psi_m(t_{n+1}) = 2\tilde{\psi}_m(t_n) - \tilde{\psi}_m(t_{n-1}) . \quad (A8)$$

In Eq. (A8), $\tilde{\psi}_m(t_n)$ and $\tilde{\psi}_m(t_{n-1})$ denote the wave functions which can be obtained by the unitary transformations in the respective subspaces spanned by $\{\psi_m(t_n)\}$ and $\{\psi_m(t_{n-1})\}$, so as to minimize the difference between two sets of wave functions $S \equiv \sum_m f_m||\tilde{\psi}_m(t_n) - \tilde{\psi}_m(t_{n-1})||^2$.[26] In addition to the wave functions, the charge density for the initial guess is also extrapolated to first order,

$$\rho(t_{n+1}) = 2\rho(t_n) - \rho(t_{n-1}) . \quad (A9)$$

By these extrapolations we can reduce the average number of iterations: Two to four iterations were used in our calculations.

[1] S. Kambayashi and G. Kahl, Phys. Rev. A **46**, 3255 (1992).

[2] U. Balucani, A. Torcini, and R. Vallauri, Phys. Rev. B **47**, 3011 (1993).

[3] K. Hoshino, H. Ugawa, and M. Watabe, J. Phys. Soc. Jpn. **61**, 2182 (1992).

[4] P. H. K. de Jong, P. Verkerk, and L. A. de Graaf, J. Non-Cryst. Solids **156-158**, 48 (1993).

[5] C. Morkel, C. Gronemeyer, W. Gläser, and J. Bosse, Phys. Rev. Lett. **58**, 1873 (1987).

[6] R. Winter, C. Pilgrim, and F. Hensel, J. Phys. (Paris) IV

1, C5-45 (1991).

[7] T. Bodensteiner, C. Morkel, W. Gläser, and B. Dorner, Phys. Rev. A **45**, 5709 (1992).

[8] F. Shimojo, K. Hoshino, and M. Watabe, J. Phys. Soc. Jpn. **63**, 141 (1994).

[9] F. Shimojo, K. Hoshino, and M. Watabe, J. Phys. Soc. Jpn. **63**, 1821 (1994).

[10] R. Car and M. Parrinello, Phys. Rev. Lett. **55**, 2471 (1985).

[11] M. C. Payne, M. P. Teter, D. C. Allan, T. A. Arias, and J. D. Joannopoulos, Rev. Mod. Phys. **64**, 1045 (1992).

[12] G.-X. Qian, M. Weinert, G. W. Fernando, and J. W. Davenport, Phys. Rev. Lett. **64**, 1146 (1990).

[13] D. M. Bylander and L. Kleinman, Phys. Rev. B **45**, 9663 (1992).

[14] J. Theihaber, Phys. Rev. B **46**, 12 990 (1992).

[15] D. L. Lynch, N. Troullier, J. D. Kress, and L. A. Collins, J. Chem. Phys. **101**, 7048 (1994).

[16] M. Foley, E. Smargiassi, and P. A. Madden, J. Phys. Condens. Matter **6**, 5231 (1994).

[17] B. J. C. Cabral and J. L. Martins, Phys. Rev. B **51**, 872 (1995).

[18] G. Franz, W. Freyland, W. Gläser, F. Hensel, and E. Schneider, J. Phys. (Paris) Colloq. **41**, C8-194 (1980).

[19] R. D. Mountain, J. Phys. F **8**, 1637 (1978).

[20] M. Tanaka, Suppl. Prog. Theor. Phys. **69**, 439 (1980); J. Phys. F **10**, 2581 (1980).

[21] G. Kahl, S. Kambayashi, and G. Nowotny, J. Non-Cryst. Solids **156-158**, 15 (1993).

[22] N. Matsuda, H. Mori, K. Hoshino, and M. Watabe, J. Phys. Condens. Matter **3**, 827 (1991).

[23] P. Hohenberg and W. Kohn, Phys. Rev. **136**, B864 (1964); W. Kohn and L. J. Sham, *ibid.* **140**, A1133 (1965).

[24] M. P. Teter, M. C. Payne, and D. C. Allan, Phys. Rev. B **40**, 12 255 (1989).

[25] D. M. Bylander, L. Kleinman, and S. Lee, Phys. Rev. B **42**, 1394 (1990).

[26] T. A. Arias, M. C. Payne, and J. D. Joannopoulos, Phys. Rev. B **45**, 1538 (1992).

[27] T. A. Arias, M. C. Payne, and J. D. Joannopoulos, Phys.

Rev. Lett. **69**, 1077 (1992).

[28] G. Kresse and J. Hafner, Phys. Rev. B **49**, 14 251 (1994).

[29] Y. Zempo, M. Ishida, and M. Yoshida, J. Mol. Struc. **310**, 17 (1994).

[30] R. D. King-Smith and D. Vanderbilt, Phys. Rev. B **49**, 5828 (1994).

[31] A. Fukumoto (unpublished).

[32] M. J. Gillan, J. Phys. Condens. Matter **1**, 689 (1989).

[33] M. Weinert and J. W. Davenport, Phys. Rev. B **45**, 13 709 (1992).

[34] R. M. Wentzcovitch, J. L. Martins, and P. B. Allen, Phys. Rev. B **45**, 11 372 (1992).

[35] N. D. Mermin, Phys. Rev. **137**, A1441 (1965).

[36] N. Troullier and J. L. Martins, Phys. Rev. B **43**, 1993 (1991).

[37] L. Kleinman and D. M. Bylander, Phys. Rev. Lett. **48**, 1425 (1982).

[38] D. M. Ceperley and B. J. Alder, Phys. Rev. Lett. **45**, 566 (1980); J. P. Perdew and A. Zunger, Phys. Rev. B **23**, 5048 (1981).

[39] S. G. Louie, S. Froyen, and M. L. Cohen, Phys. Rev. B **26**, 1738 (1982).

[40] S. Nosé, Mol. Phys. **52**, 255 (1984).

[41] W. G. Hoover, Phys. Rev. A **31**, 1695 (1985).

[42] Y. Waseda, *The Structure of Non-crystalline Materials* (McGraw-Hill, New York, 1980).

[43] D. N. Theodorou and U. W. Suter, J. Chem. Phys. **82**, 955 (1985).

[44] *Handbook of Thermodynamic and Transport Properties of Alkali Metals*, edited by R. W. Ohse (Oxford, Blackwell, 1985).

[45] K. Hoshino and M. Watabe, J. Phys. Soc. Jpn. **61**, 1663 (1992).

[46] S. Takeda, S. Tamaki, and Y. Waseda, J. Phys. Condens. Matter **2**, 6451 (1990).

[47] G. P. Kerker, Phys. Rev. B **23**, 3082 (1981).

[48] See, for example, W. E. Pickett, Comput. Phys. Rep. **9**, 115 (1989).